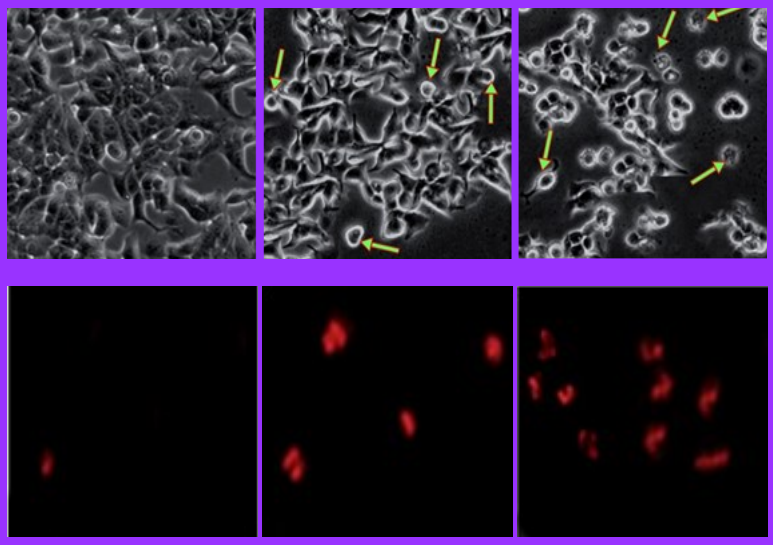

BJP

Bangladesh Journal of Pharmacology

Research Article

Cytotoxic effect of *Luffa cylindrica* leaf extract on MCF-7 cell lines

A Journal of the Bangladesh Pharmacological Society (BDPS)
Journal homepage: www.bdpsjournal.org; www.banglajol.info
Abstracted/indexed in Academic Search Complete, Agroforestry Abstracts, Asia Journals Online, Bangladesh Journals Online, Biological Abstracts, BIOSIS Previews, CAB Abstracts, Current Abstracts, Directory of Open Access Journals, EMBASE/Excerpta Medica, Global Health, Google Scholar, HINARI (WHO), International Pharmaceutical Abstracts, Open J-gate, Science Citation Index Expanded, SCOPUS and Social Sciences Citation Index
ISSN: 1991-0088

Bangladesh J Pharmacol 2025; 20: 101-112

Cytotoxic effect of *Luffa cylindrica* leaf extract on MCF-7 cell lines

Hanzla Arshad and Mohammad Saleem

Department of Pharmacy, University College of Pharmacy, University of the Punjab, Lahore, Pakistan.

Article Info

Received: 17 May 2025
Accepted: 14 July 2025
Available Online: 31 August 2025

DOI: 10.3329/bjp.v20i3.81752

Cite this article:
Arshad H, Saleem M. Cytotoxic effect of *Luffa cylindrica* leaf extract on MCF-7 cell lines. Bangladesh J Pharmacol. 2025; 20: 101-112.

Abstract

This study investigated the cytotoxic effect of *Luffa cylindrica* leaf aqueous ethanolic extract on breast cancer cell lines MCF-7 and the normal epithelial cell line MCF-10A. Phytochemical screening and DPPH assays confirmed the presence of antioxidant compounds. MTT showed a dose-dependent reduction in cancer cell viability ($p<0.05$), with minimal effects on MCF-10A. Doxorubicin, in contrast, was toxic to MCF-7 cell lines. Apoptotic cell death induced by the extract was verified through morphological analysis, annexin V-FITC binding, and Hoechst/propidium staining. The extract significantly reduced reactive oxygen species (ROS) and delayed cell migration, as observed in the scratch assay. Overall, *L. cylindrica* demonstrated selective cytotoxicity, antioxidant potential, and anti-metastatic properties, supporting its potential as a promising natural candidate for breast cancer treatment.

Introduction

Cancer remains one of the leading causes of death worldwide, with breast cancer being the most frequently diagnosed malignancy in women (Siegel et al., 2023). Chemotherapy continues to play a central role in cancer treatment (Wu et al., 2021); however, its use is limited by severe adverse effects, the development of drug resistance, and high costs (Wang et al., 2022).

A key feature of tumor progression is the ability of malignant cells to evade apoptosis— a form of programmed cell death governed by intrinsic and extrinsic signaling cascades that converge on caspase activation, leading to the dismantling of DNA and protein structures (Liu et al., 2021). By restoring or enhancing apoptotic pathways, novel anti-cancer agents can selectively eliminate cancer cells while sparing healthy tissue (Zhao et al., 2020).

The success of vincristine, derived from *Catharanthus roseus*, has interest in plant-based therapeutics as potentially safer and more cost-effective alternatives to purely synthetic drugs. *Luffa cylindrica*, long used in traditional medicine to treat conditions such as sinusitis, asthma, helminth infections, bronchitis, and localized inflammation (Alam et al., 2023), attracted attention for its antitumor activity (Guan et al., 2021).

Phytochemical analyses of *L. cylindrica* have identified a suite of bioactive phenolics—quercetin, gallic acid, caffeic acid, benzoic acid, p-coumaric acid, ferulic acid, cinnamic acid, and kaempferol (Khan et al., 2022)—that exhibit cytotoxic effects by inducing apoptosis and inhibiting angiogenesis, metastasis, and proliferation. Additional studies have documented antioxidant, antibacterial, anti-diabetic, and cytotoxic activities of *L. cylindrica in vitro* (Bulbul et al., 2011; Sola et al., 2021; Funmilayo et al., 2021; Indurthi and Sarma, 2024; Garai et al., 2018). Cucurbitacin B, a triterpenoid glycoside isolated from *L. cylindrica*, induces apoptosis in various human cancer cell lines via caspase-3 and caspase-9 activation and suppresses tumor-promoting JAK2/STAT3 signaling (Samra, 2018; Duangmano et al., 2012). For example, quercetin activates caspase-3, induces

This work is licensed under a Creative Commons Attribution 4.0 License. You are free to copy, distribute and perform the work. You must attribute the work in the manner specified by the author or licensor.

autophagy-associated cell death (Zhou et al., 2021), and gallic acid suppresses the growth of malignant cells while promoting apoptosis (Islam et al., 2023). Similarly, p-coumaric acid causes cell-cycle arrest and tumor regression in preclinical models (Tan et al., 2020); ferulic acid downregulates pro-survival genes to arrest cells in G_1 phase (Kang et al., 2024); and cinnamic acid derivatives generate reactive oxygen species (ROS) that inflict irreversible DNA damage (Zheng et al., 2008).

Accordingly, this study aims to evaluate the cytotoxic, anti-metastatic, and pro-apoptotic effects of *L. cylindrica* extract on selected cancer cell lines.

Materials and Methods

Chemicals

Quercetin, kaempferol, gallic acid, ferulic acid, benzoic acid, p-coumaric acid, caffeic acid, cinnamic acid, DMEM, and fetal bovine serum were purchased from Sigma-Aldrich, USA. HPLC-grade acetonitrile was purchased from Merck, Germany. The ROS detection assay kit was purchased from Thermo Fisher Scientific, USA.

Preparation of extract

Approximately 30 kg of dried *L. cylindrica* leaves were milled into a fine powder. This powder was then macerated in a 70:30 (v/v) ethanol-water mixture for seven days at room temperature, with intermittent stirring to facilitate the extraction of both polar and semi-polar constituents (Alam et al., 2023). After maceration, the suspension was first passed through a No. 16 mesh (0.0445 mm) to remove coarse debris. The crude filtrate was further clarified by sequential filtration through Whatman paper (11 µm pore size) and a 0.22 µm syringe filter to eliminate fine particulates and ensure sterility.

The clarified extract was concentrated to dryness in a hot-air oven maintained at 45 °C— an optimized temperature that preserves thermolabile phytochemicals while evaporating the solvent (Zhou et al., 2021). The resulting crude extract was grounded to a uniform powder, accurately weighed, and stored in sterile glass vials at –20°C until use, thereby maintaining chemical integrity and preventing microbial growth (Islam et al., 2023).

Preparation of stock solution

The extract was dissolved in 100% ethanol to prepare a 10 mg/mL stock solution. This stock solution was further diluted to obtain a working stock solution (1 mg/mL).

Determination of antioxidant properties

DPPH assay

The sample's antioxidant properties were evaluated using the DPPH (2,2-diphenyl-1-picrylhydrazyl) free radical assay. DPPH is a stable purple-colored free radical that turns yellow upon reduction by antioxidant compounds, serving as a widely accepted method for determining total antioxidant capacity (TAC) (Blois, 1958). This method assesses the collective ability of a substance to neutralize ROS by measuring the IC_{50} value— the concentration required to scavenge 50% of the DPPH radicals. A lower IC_{50} value indicates stronger antioxidant capacity, whereas a higher value denotes weaker activity (Rafiq et al., 2023). IC_{50} was calculated through linear regression analysis using Microsoft Excel 2016.

In this study, the DPPH solution was prepared by dissolving 4 mg of DPPH in 100 mL of ethanol (0.004% w/v). Equal volumes of DPPH solution and varying concentrations of *L. cylindrica* extract were mixed in labeled test tubes. The tubes were incubated in the dark at room temperature, and the absorbance was measured at 517 nm using a NANBEI UV-visible spectrophotometer (Model NU-T3A, China). The decrease in absorbance observed visually as the color changes from purple to yellow indicates the degree of free radical scavenging by the extract (Bibi et al., 2021).

The plant extract was tested at ethanol concentrations of 10 to 100 µg/mL. The percentage of free radical scavenging activity was calculated using the standard formula. The IC_{50} was derived from the plotted inhibition curve to assess antioxidant potency (Zhang et al., 2020).

%Inhibition = [(Absorbance of control – Absorbance of test solution) / Absorbance of control] × 100

Measurement of ROS

The ROS detection assay kit was used to evaluate the effects of *L. cylindrica* extract on intracellular ROS levels in breast cancer cells. The assay employs 2',7'-dichlorofluorescin diacetate (DCFDA), a cell-permeable, non-fluorescent probe that becomes fluorescent upon oxidation. Once inside the cell, DCFDA is deacetylated by intracellular esterases to form DCFH, which is subsequently oxidized by ROS into 2',7'-dichlorofluorescein (DCF), a highly fluorescent compound (Iqbal et al., 2021).

MCF-7 cells were seeded into 96-well plates at a density of 4×10^4 cells/well and incubated overnight to allow cell adherence. The next day, following media removal, the cells were incubated with 25 µM DCFDA for 45 min in the dark at 37°C. After incubation, the cells were gently washed with buffer to remove excess dye.

Subsequently, three wells per treatment group were exposed to *L. cylindrica* extract at 20 and 40 µg/mL for MCF-7 cells. The cells were incubated for 3 hours at 37° C with 5%CO_2. The experimental design also included a positive control, an untreated (vehicle) control, and

Box 1: Scratch assay

Principle

The scratch assay (wound healing assay) is used to assess cell migration and the ability of cells to close a wound or scratch in a confluent monolayer.

Requirements

Cell culture plates (e.g., 6-well plates); Cancer cell lines MCF-7; *L. cylindrica* leaf extract; Complete growth media (e.g., RPMI -1640, DMEM); Sterile pipette tips; Sterile pipette; Microplate reader or phase contrast microscope for imaging; Incubator at 37°C with 5%CO_2

Procedure

Step 1: Seed the cells in a 6-well plate and allow them to grow until they form a confluent monolayer.

Step 2: Use a sterile pipette tip or a suitable mechanical device to create a scratch or wound in the monolayer.

Step 3: Wash the cells gently with PBS (phosphate-buffered saline) to remove any detached cells.

Step 4: Add fresh media with or without *L. cylindrica* leaf extract to the cells.

Step 5: Incubate the cells at 37°C with 5% CO_2.

Step 6: Capture images of the scratch area at regular intervals (e.g., 0, 24, 48 hours) using a phase contrast microscope to monitor cell migration.

Step 7: Measure the wound closure by calculating the area of the gap at each time point and comparing it with the initial scratch size.

Step 8: Analyze the results to determine if the *L. cylindrica* leaf extract affects cell migration, which would suggest anti-metastatic properties.

Reference

Nadeem et al., 2023

blank wells.

Fluorescence intensity was measured using a Varioskan ALF multimode fluorescent microplate reader (Thermo Fisher Scientific, USA) with excitation at 485 nm and emission at 535 nm. Background and blank values were subtracted from all readings, and ROS generation was calculated as a percentage relative to the untreated control group.

HPLC (High-performance liquid chromatography)

An extract sample (50 mg) was taken and dissolved in methanol (24 mL). The solution was homogenized, then distilled water (16 mL) and 6M hydrochloric acid (10 mL) were added. The mixture was heated at 95 °C for 2 hours using a thermostat. Afterwards, the final solution was filtered through a nylon membrane filter (0.45 µm, Millipore, USA) before HPLC analysis.

For chromatographic separation, a Shimadzu LC-10A system was used with a Shim-pack CLC-ODS C18 column (Shimpack CLC-ODS C18 column). Mobile phase A consisted of water adjusted to pH 2.27 with acetic acid, and mobile phase B was HPLC-grade acetonitrile. The gradient began with mobile phase B at 15%, rose to 45% over 15 min, then to 100% at 35 min, and was maintained until 45 min. Phenolic compounds were detected with a UV–Vis detector set at 280 nm. Identity confirmation was done by comparing retention times and UV spectra to those of standards. The procedure was conducted at ambient temperature.

Fourier-Transform Infrared (FTIR) spectroscopy of L. cylindrica extract

Dried *L. cylindrica* crude extract (2 mg) was finely ground with 200 mg of spectroscopic-grade potassium bromide in a mortar and pestle until a homogeneous mixture was obtained. The mixture was then loaded into a 13 mm die and compressed at 10 tonnes for 2 min using a hydraulic press to form a transparent pellet. FTIR spectra were recorded on a PerkinElmer Spectrum Two spectrometer over the 4000–400 cm^{-1} range, with a spectral resolution of 4 cm^{-1} and 32 scans per sample to improve the signal-to-noise ratio. A pure potassium bromide pellet spectrum was collected under identical conditions and automatically subtracted as background. Key absorption bands were assigned by comparison with standard spectral libraries to identify functional groups characteristic of phenolics, flavonoids, and other bioactive constituents (Amin and Mohamed, 2021).

LCMS

Dried *L. cylindrica* leaf extract (50 mg) was dissolved in 1 mL of HPLC-grade methanol, followed by vigorous vortexing for five minutes to ensure thorough dissolution. The mixture was allowed to sonicate for 15 min in an ice-water bath to facilitate the complete extraction of phytochemicals. Subsequently, the sample was centrifuged at 12,000 × g for 10 min at 4°C. The clear supernatant was carefully transferred into a new vial and filtered through a 0.22 µm PTFE syringe filter into an LC-MS autosampler vial to eliminate any particulate matter.

Chromatographic separation was conducted using an Agilent 1290 Infinity II UHPLC system equipped with a zorbax eclipse plus C18 column (2.1 × 100 mm, 1.8 µm). The column temperature was maintained at 40°C. The mobile phase consisted of solvent A (0.1% formic acid in water) and solvent B (0.1% formic acid in acetonitrile), delivered at a flow rate of 0.3 mL/min. Initially equilibrated with solvent B at 5% for 2 min, the gradient was linearly increased to 95% over the subsequent 18 min, held at 95% for an additional 2 min, and finally re-equilibrated back to 5% for the last 2 min. A 5 µL aliquot of the filtered extract was injected per analytical run.

Mass spectrometry was conducted using an Agilent 6545 Q-TOF LC-MS system employing electrospray

ionization in both positive and negative modes. Drying gas (300°C, 8 L/min) and sheath gas (350°C, 11 L/min) flows were optimized for maximal ion desolvation, with capillary voltages at ± 3 kV and a fragment voltage of 175 V. Mass scans were performed over an m/z range of 50–1700 at a rate of 2 spectra/sec. Data-dependent MS/MS fragmentation was conducted on the three most abundant precursor ions per cycle at collision energies of 10, 20, and 40 eV.

Raw data processing was done using Agilent mass-Hunter qualitative analysis software. Automated peak detection was used with tolerances of ± 5 ppm mass accuracy and ± 0.2 min retention time. Compound identification was done by comparing accurate masses and MS/MS fragmentation patterns against the METLIN and MassBank databases. Additionally, the identities of major constituents were validated through direct comparison with commercially sourced authentic standards.

Cell lines

All cell lines were sourced from the Center of Excellence in Molecular Biology, University of the Punjab. All cell lines were cultured in DMEM having 10%fetal bovine serum and 1%antibiotic solution (penicillin and streptomycin). To cultivate these cell lines, cell culture-treated flasks were kept in an incubator adjusted to 37° C with 5%CO_2 concentration. Regular microscopic examination was performed to identify any signs of contamination. Sub-culturing was done to sustain the cells when they reached a confluence level of around 70-80%. The DMEM medium was refreshed every 2 to 3 days.

Previous media was discarded. PBS (phosphate-buffered saline) was added to rinse the cells. PBS was removed, and 3 mL of trypsin/EDTA was added, and placed in an incubator at 37°C. Upon cell detachment, 7 mL DMEM with 10%fetal bovine serum was added in a small amount to inactivate trypsin. Pipetting was done to disperse the cells properly. After cell counting, 375,000 cells were transferred to a fresh T75 flask. This flask was then placed in an incubator at 37°C with 5% CO_2 till the completion of the monolayer.

The process of cell enumeration was conducted using a hemocytometer. Initially, the culture media were discarded, and the cells were washed with PBS to remove any residual serum. Following this, the PBS was removed, and trypsinization was carried out to detach the adherent cells. After successful cell detachment, 5 mL of media containing 10%fetal bovine serum was added to inactivate the trypsin. A portion of the media containing the suspended cells (200 µL) was transferred into an Eppendorf tube using a micropipette.

After cleaning the hemocytometer and coverslip according to standard protocol, 100 µL of the cell suspension was introduced to each chamber of the hemocytometer. Once the cells had settled, counting was performed in four corner squares under a microscope. The final cell concentration was calculated using the standard hemocytometer formula (Khan et al., 2021).

Number of cells per mL of media = Average number of cells in 4 squares × 10^4

Whereas, 10^4 is the dilution factor

MTT assay

A 96-well plate was used for the cell viability assay. Cells were seeded at a density of 10,000 cells per well for the respective cell line (Rahman et al., 2022). The plate was then incubated at 37°C in a 5%CO_2 incubator for 24 hours. After incubation, cell growth was examined under an inverted microscope. The plant extract was subsequently added in triplicate at two-fold serial dilutions with the following concentrations: 0.78, 1.56, 3.12, 6.25, 12.5, 25, and 50 µg/mL.

Doxorubicin, a standard anti-cancer drug, was added to each cell line at the same concentrations used for *L. cylindrica* extract for comparison. The treated cells were further incubated for 48 hours.

After incubation, MTT solution (50 µL) was added to each well. The plate was placed in a CO_2 incubator (37° C, 5%CO_2) and kept in the dark for 2 hours to allow formazan crystals to form. The medium was then removed, and 100 µL of DMSO was added to dissolve the formazan. Plates were gently agitated at room temperature for 15 min to ensure complete solubilization.

Absorbance was measured at 570 nm using an ELISA plate reader (Model RT-6000, Rayto, Germany). Cell viability (%) was calculated using the standard formula. The IC_{50} value (concentration causing 50% inhibition of cell viability) was determined by linear regression analysis using Microsoft Excel 2016.

%Cell viability = A_{570} of treated cells-blank A_{570} of untreated cells − blank × 100

Phase contrast microscopy of cell morphology

Cells were seeded at 1×10^5 per well in a 24-well plate and allowed to adhere overnight. After removing the spent medium, cells were treated with *L. cylindrica* extract at concentrations of 10, 20, and 40 µg/mL for MCF-7. Plates were incubated for 24 hours at 37 °C in 5%CO_2. An untreated control was included. Morphological alterations were evaluated under an inverted light microscope using a 100x objective.

Detection of apoptosis using annexin V

Phosphatidylserine externalization, a hallmark of early apoptosis, was assessed using annexin V-FITC, a fluorescent dye that binds specifically to phosphatidylserine and emits green fluorescence upon excitation. In the early stages of apoptosis, phosphatidylserine translocates from the inner to the outer leaflet of the plasma

membrane, allowing annexin V to bind, and indicate the apoptotic initiation (Hameed et al., 2022).

MCF-7 breast cancer cell lines were seeded on sterile coverslips and incubated for 24 hours. Afterward, they were treated with *L. cylindrica* extract at 20 and 40 µg/mL for MCF-7 cells, and incubated for another 24 hours at 37°C in 5%CO_2.

Following treatment, cells were stained with annexin V-FITC, according to the manufacturer's protocol. Stained cells were then visualized under a fluorescence microscope, and green fluorescence indicated early apoptotic cells, confirming the extract's role in inducing apoptosis.

Microscopic nuclear analysis by Hoechst/ propidium iodide staining

Hoechst 33342 is a cell-permeable dye that binds to DNA and was capable of staining the nuclei of both live and dead cells. In contrast, propidium iodide cannot permeate intact cell membranes and is commonly used to selectively stain non-viable cells, making the combination of these dyes a reliable method for identifying apoptotic and necrotic cells (Farooq et al., 2021).

For this experiment, 1 × 10^5 cells of MCF-7 were seeded in 24-well plates. After overnight incubation at 37°C in a CO_2-enriched environment, MCF-7 cells were treated with *L. cylindrica* extract at 20 and 40 µg/mL. The treated cells were further incubated for 24 hours at 37°C in a humidified 5%CO_2 incubator.

Post-incubation, the culture medium was removed and the cells were washed gently with PBS. Staining was initiated by adding Hoechst 33342 (10 µg/mL) to each well, followed by a 10-min incubation in the dark at 37°C. Subsequently, propidium iodide (2.5 µg/mL) was added to the wells, and the plates were kept in the dark at room temperature for 5 min. After a final PBS wash, the cells were visualized using a fluorescent inverted microscope. Live and apoptotic cells were distinguished based on nuclear morphology, where condensed or fragmented nuclei indicated apoptosis.

Scratch assay (wound healing assay)

The scratch assay is a widely used and straightforward technique for monitoring the migration of cancer cells *in vitro*. In this assay, adherent cancer cells are treated with the *L. cylindrica* extract and incubated briefly (1–2 hours), followed by the creation of a mechanical scratch using a sterile pipette tip or needle. The scratch width is then measured at different time intervals to evaluate cell migration. This method can also assess the impact of a test compound on cellular invasiveness. A low-serum medium (1%) is used to limit proliferation and accurately quantify migration, while higher serum concentrations are employed in proliferation studies (Ahmed et al., 2023).

A 6-well tissue culture plate was used. All materials were sterilized appropriately before the experiment. Cells were seeded at a density of 1.75 × 10^5 cells/mL, and 2 mL of medium was added to each well for both MCF-7 cell lines. An equal numbers of cells were dispensed into each well and incubated at 37°C in a 5% CO_2 incubator to allow attachment.

Once cells adhered, the plate was removed from the incubator, and the medium was carefully aspirated and replaced with a low-serum (1%) medium to reduce proliferation. Care was taken to avoid disturbing the monolayer by tilting the plate and aspirating from the side using a suction tip. To inhibit cell proliferation and confirm that scratch closure results only from migration, mitomycin C was added.

Three wells per cell line were treated with *L. cylindrica* extract at their respective IC_{50} concentrations, while the other three served as untreated controls. After adding the treatments, the plate was incubated for 2 hours.

A scratch was created using a 200 µL pipette tip, held like a pencil, to gently scrape a line through the cell monolayer. The plate was immediately observed under an inverted microscope, showing clear scratch boundaries and a cell-free zone in the center.

Images of the scratch were captured at various time points post-scratch to monitor closure. The scratch area was quantified using ImageJ software (version 1.54g). The following formula was applied to estimate the scratch closure percentage:

$$\text{Scratch closure } \% = (A_0 - A_i)A_0 \times 100$$

Where, A_0 is the scratch area immediately after wounding (time 0), A_i is the scratch area at the given post-scratch time point

Statistical analysis

The experimental data were reported using the mean ± standard deviation (SD). Graph pad prism 8.0.1 and Microsoft Excel 2016 were used to analyze data. Linear regression analysis was used to measure IC_{50} values of the cell lines used. T-test was used to compare values of *L. cylindrica* and doxorubicin for each cell line to determine whether it is significant or not having p value <0.05 considered significant.

Results

DPPH assay

Both *L. cylindrica* and ascorbic acid possess antioxidant activity in a dose-dependent manner. Results indicated that *L. cylindrica* exhibited less antioxidant activity than ascorbic acid (Table I). IC_{50} values of *L. cylindrica* and ascorbic acid were 890 µg/mL and 154 µg/mL, respectively.

Table I

Scavenging ability of *L. cylindrica* extract and ascorbic acid

Equal concentrations (µg/mL) of extract and DPPH	%Inhibition	
	L. cylindrica extract	Ascorbic acid
10	1.2	5.2
20	1.9	8.7
30	2.6	11.9
40	3.8	13.5
50	4.0	17.3
60	4.7	19.9
70	5.1	22.0
80	5.6	26.1
90	5.9	30.9
100	6.0	34.2

Effect on intracellular ROS levels

ROS are produced within cells in response to a variety of stress conditions. Natural products can reduce the level of ROS in normal cells. Non-fluorescent DCFDA oxidation to fluorescent DCF was counted in the treated cells to ascertain whether *L. cylindrica* reduces the levels of ROS in cancerous cells (Figure 1). *L. cylindrica* reduces the levels of ROS in a concentration-dependent manner.

Quantitative analysis of phytochemicals

The HPLC analysis of *L. cylindrica* leaf extract identified several bioactive compounds and quantified their concentrations. Quercetin was the most abundant compound, with a concentration of 101.9 ppm, comprising 22.7% of the total area. The extract also contained significant amounts of ferulic acid at 10.7 ppm (1.8%), and kaempferol, which was the second most prominent compound, at 811.4 ppm, accounting for 46.4% of the total area. Benzoic acid was detected at 8.5 ppm (0.9%), followed by gallic acid at 3.46 ppm (1.1%), cinnamic acid at 0.7 ppm (0.7%), and caffeic acid at 0.7 ppm (0.2%). p-Coumaric acid had the lowest concentration at 0.15 ppm (0.1%). These findings indicate a rich phytochemical profile in the extract, particularly high in kaempferol and quercetin, suggesting its potential therapeutic applications (Figure 2).

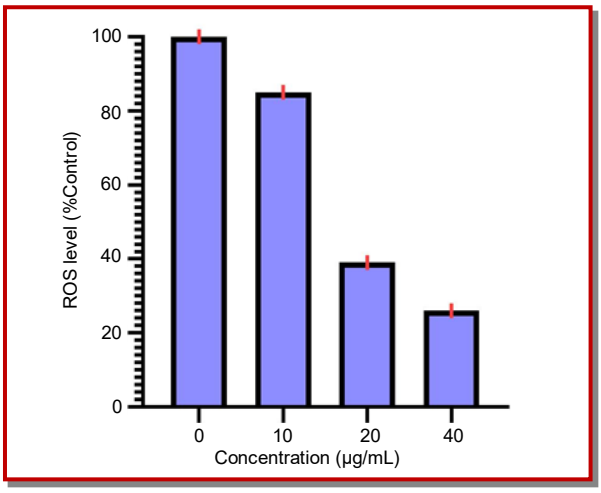

Figure 1: Effect of *L. cylindrica* extract on intracellular ROS levels on MCF-7 cells. The graph represents the mean ROS levels as a percentage of the control, where ROS levels in untreated cells were set to 100%. Data are mean ± SD; n=3

FTIR result

FTIR analysis of the *L. cylindrica* extract revealed distinctive absorption bands corresponding to specific functional groups indicative of its phytochemical composition. A broad absorption band at approximately 3300 cm^{-1} signified hydrogen-bonded O–H stretching typical of hydroxyl groups in phenolic compounds. Medium intensity bands observed at 2920 and 2850 cm^{-1} were attributed to aliphatic C–H stretching vibrations, suggesting the presence of CH_2 and CH_3 groups associated with terpenoid structures. A sharp absorption peak at 1710 cm^{-1} was characteristic of conjugated carbonyl (C=O) groups, likely present in ketones or carboxylic acids. Aromatic ring vibrations were indicated by the band at 1620 cm^{-1}, while aromatic C–H bending was evident at 1510 cm^{-1}. The medium band at 1430 cm^{-1} corresponded to phenolic O–H bending. Bands between 1260 and 1240 cm^{-1} represent C–O stretching vibrations typically found in aryl ethers and phenolic esters. Strong absorption at 1100 cm^{-1} indicates C–O–C vibrations, consistent with glycosidic linkages in flavonoid glycosides. Weak bands within the range of 950–900 cm^{-1} signified out-of-plane aromatic C–H bending. These observations collectively confirmed the presence of phenolic acids, flavonoids, glycosides, and minor terpenoid components within the extract (Table II).

LC–MS analysis

LC–MS analysis of the *L. cylindrica* leaf extract verified the presence of eight prominent phenolic and flavonoid constituents, each precisely identified through accurate mass measurements, MS/MS fragmentation patterns, and comparison to authentic chemical standards. Kaempferol ($[M-H]^-$ m/z 285.04) and quercetin ($[M-H]^-$ m/z 301.0) were the dominant constituents, constituting 45.8% and 23.1% of the total peak area, respectively (Table III). Gallic acid (m/z 169.0), ferulic acid (m/z 193.1), and benzoic acid (m/z 121.0) were observed in lower abundances of 1.2%, 1.9%, and 0.9%, respectively. Trace quantities (<1%) of caffeic acid (m/z 179.0), p-coumaric acid (m/z 163.0), and cinnamic acid (m/z 147.1) were also detected.

Retention times, aligned against standards under identical chromatographic conditions, were recorded as follows: gallic acid (1.8 min), benzoic acid (2.6 min), caffeic acid (3.4 min), p-coumaric acid (4.1 min), quer-

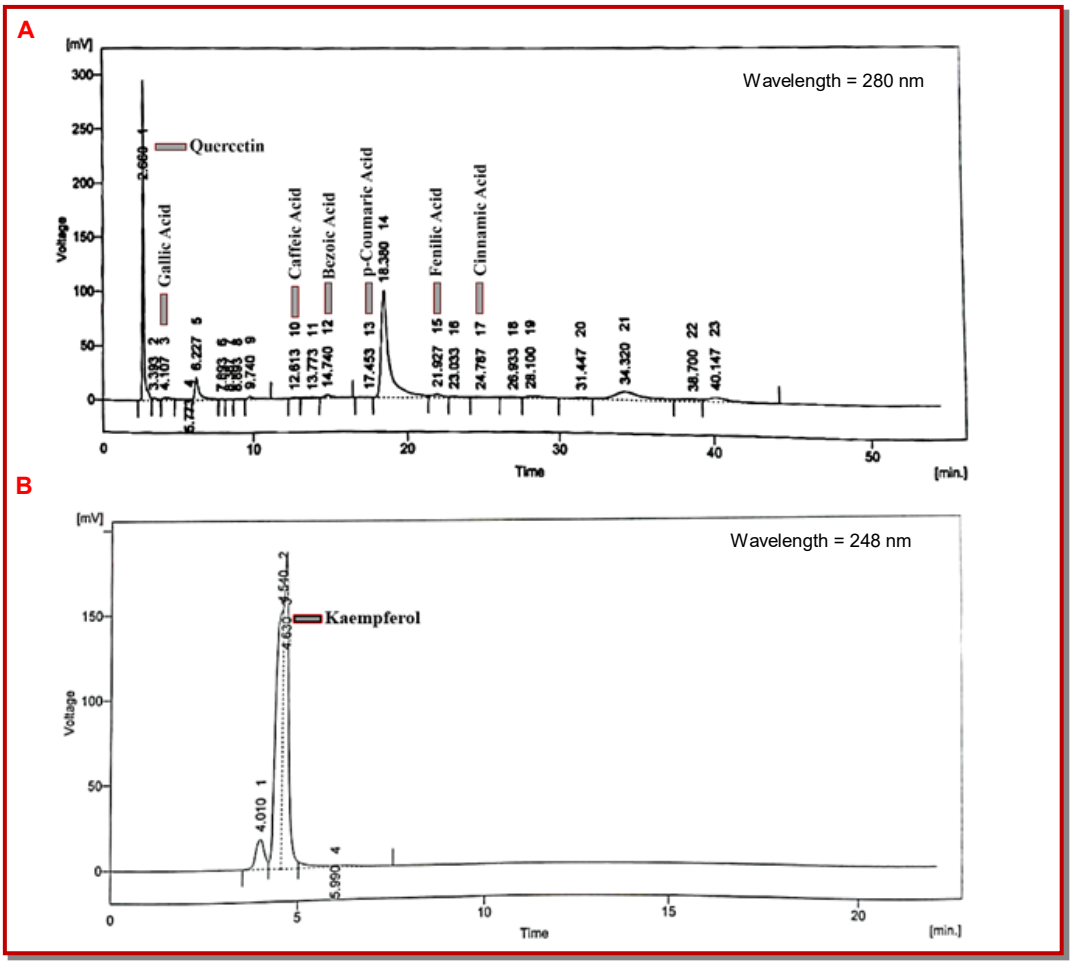

Figure 2: HPLC data of *L. cylindrica* leaf extract at two different wavelengths [upper peaks at 280 nm (A); lower peaks at 248 nm (B)] to visualize all compounds

Table II

FTIR bands and assignments

Wavenumber (cm^{-1})	Band shape	Functional-group assignment
~3300	Broad	O–H stretching (hydrogen-bonded hydroxyls in phenolics)
2920, 2850	Medium	Aliphatic C–H stretching (CH_2, CH_3 moieties)
1710	Sharp	C=O stretching (conjugated ketone/carboxylic acid)
1620	Medium	Aromatic C=C ring vibrations
1510	Medium	Aromatic C–H bending (polyphenol backbone)
1430	Medium	Phenolic O–H bending
1260–1240	Medium	C–O stretching (aryl ethers, phenolic esters)
1100	Strong	C–O–C vibration (glycosidic linkages in flavonoid glycosides)
950–900	Weak	Out-of-plane aromatic C–H bending

cetin (5.2 min), ferulic acid (6.3 min), cinnamic acid (7.8 min), and kaempferol (8.9 min).

MTT assay

Cell viability decreased with a rise in concentration for cancerous cell lines. To compare *L. cylindrica* and doxorubicin, different but the same doses were prepared and applied to both cancerous and normal cell lines. Doxorubicin reduced cell viability more than *L. cylindrica* in MCF-7. However, doxorubicin significantly lowered cell viability in normal MCF-10A cells compared to *L. cylindrica*, which did not show any prominent effect on MCF-10A cells (Figure 3).

At concentrations ≥0.78 µg/mL, extract versus doxorubicin differences were statistically significant ($p<0.05$), indicating the extract generally reduced MCF-7 viability more than doxorubicin at matching doses. In MCF-10A non-tumorigenic cells, *L. cylindrica* extract did not reduce viability significantly more than doxorubicin, indicating that the extract was non-cytotoxic to MCF-10A cells under these conditions.

Determination of IC_{50}

Table III

LC–MS profileof major phenolic and flavonoid constituents in *L. cylindrica* leaf extract

Compound	Retention time (min)	Ion mode and m/z	Relative abundance (%)
Gallic acid	1.8	$[M-H]^-$ 169.01	1.2
Benzoic acid	2.6	$[M-H]^-$ 121.03	0.9
Caffeic acid	3.4	$[M-H]^-$ 179.03	0.2
p-Coumaric acid	4.1	$[M-H]^-$ 163.04	0.1
Quercetin	5.2	$[M-H]^-$ 301.03	23.1
Ferulic acid	6.3	$[M-H]^-$ 193.05	1.9
Cinnamic acid	7.8	$[M-H]^-$ 147.05	0.7
Kaempferol	8.9	$[M-H]^-$ 285.04	45.8

Negative ion mode

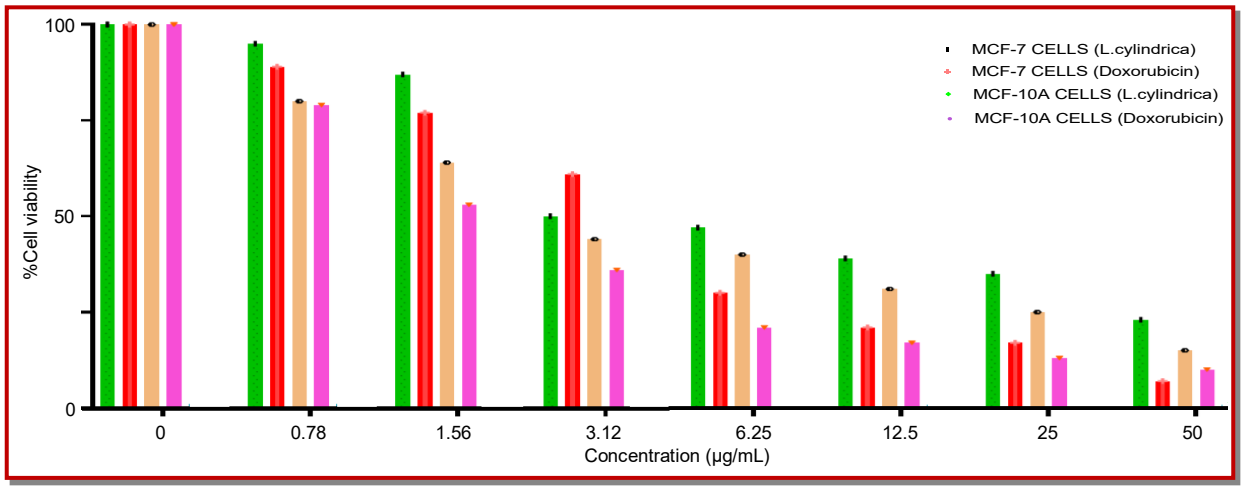

Figure 3: Dose-dependent cytotoxicity of *L. cylindrica* in MCF-7 and MCF-10A cell lines

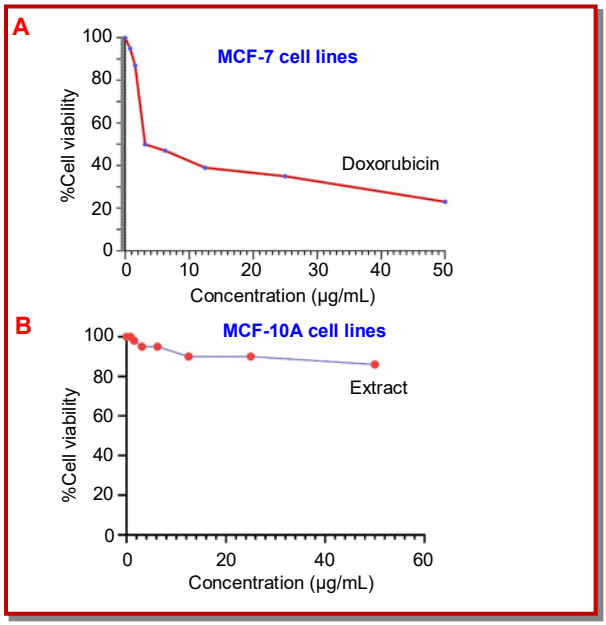

Figure 4: Comparison of percentage cell viability between *L. cylindrica* extract and doxorubicin after 48-hour treatment on MCF-7 and MCF-10A cell lines

The IC_{50} value for MCF-7 was determined to be 19.7 µg/mL, respectively. Nevertheless, this compound's cytotoxic activity was not observed in normal non-tumorigenic epithelial cell line MCF-10A cells, whose IC_{50} value was >50, which was significantly higher than that of MCF-7 (Figure 4).

Studies on apoptosis

Based on morphological characteristics: Prominent morphological alterations such as cellular shrinkage, separation, and rounding, alongside the occurrence of membrane blebbing, were observed in cancerous cell lines (Figure 5A). No peculiar difference in the morphological characteristics of MCF-10A cells was observed upon drug addition.

Annexin V FITC: The intensity of green fluorescence increased in a dose-dependent manner, indicating that *L. cylindrica* extract induced the movement of phospholipid phosphatidylserine to the outer surface of the plasma membrane. This process was responsible for initiating the beginning phase of apoptosis in MCF-7 cell lines (Figure 5B).

Hoechst 33342 staining/pripodium iodide staining: The

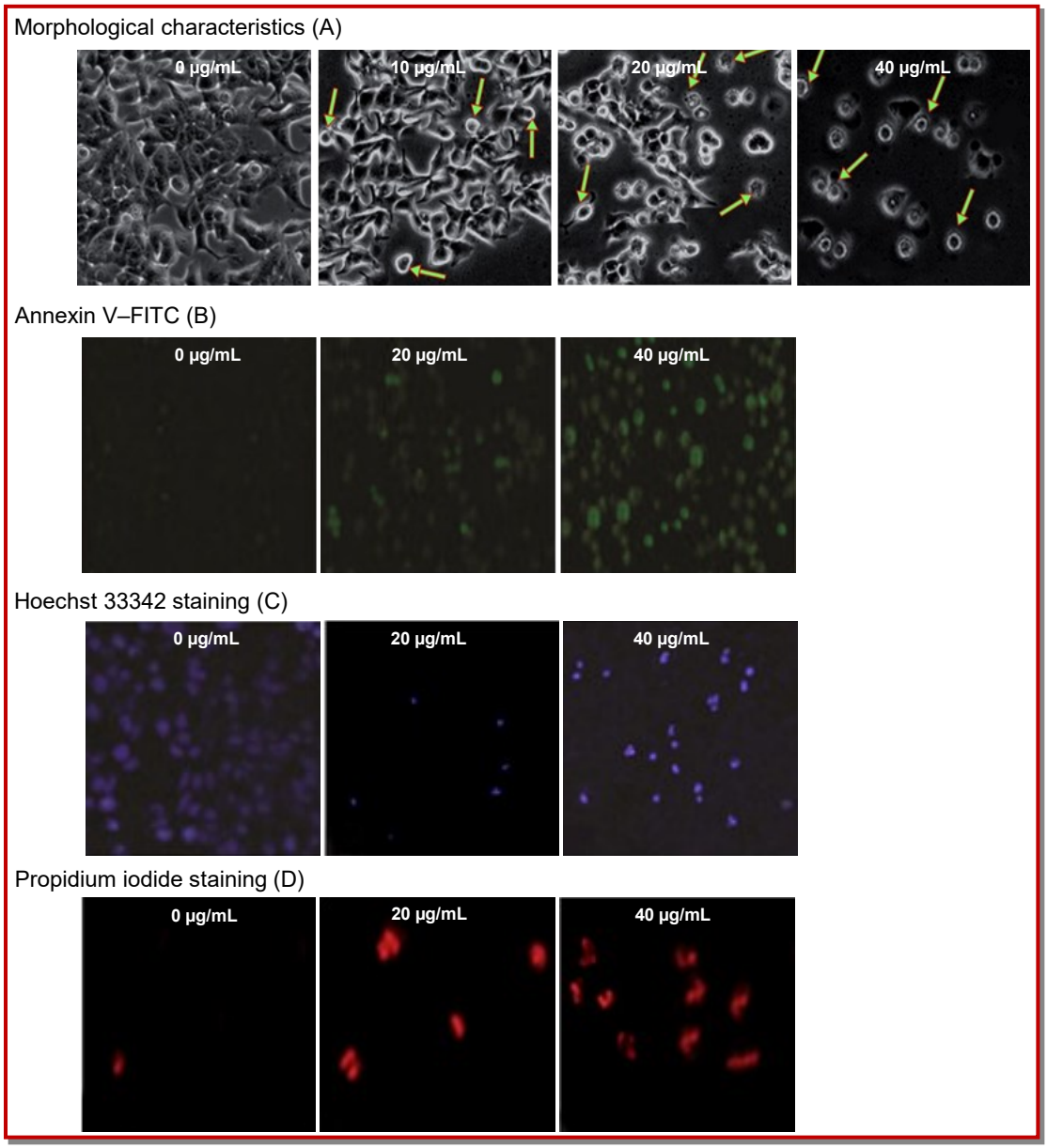

Figure 5: Apoptotic morphological characteristics (A), annexin V–FITC (B), Hoechst 33342 staining (C), and propidium iodide staining (D) of the MCF-7 cell lines were observed after 24 hour (48 hours in annexin V–FITC) exposure at 0, 10, 20, and 40 µg/mL concentrations of the *L. cylindrica* extract. Magnification 100x

apoptosis-inducing ability of *L. cylindrica* extract on cancerous cell lines was demonstrated using Hoechst 33342 staining (Figure 5C). Hoechst 33342 gave blue fluorescence by binding with the chromatin of the nucleus and made it brighter as compared to normal cells. The findings of this investigation validated that there was an elevation in fluorescence caused by chromatin condensation in cancerous cell lines, in comparison to the control group, in a way that was dependent on the dosage.

In parallel, propidium iodide staining was employed to assess cell viability. It is a DNA-binding dye that can only enter cells with compromised membranes, such as dead or late apoptotic cells. Once inside, it emits red fluorescence (Figure 5D). This allows for the differentiation between live and dead cells, with viable cells excluded from propidium iodide staining and non-viable cells displaying strong red fluorescence. The combination of Hoechst and propidium iodide staining provided a comprehensive view of cell viability and apoptosis, confirming the cytotoxic effects of the extract on cancerous cells.

Scratch assay

MCF-7 cells in which the drug was not added took 29 hours for the cells to cover the scratch-made with a sterile micropipette tip completely. However, MCF-7

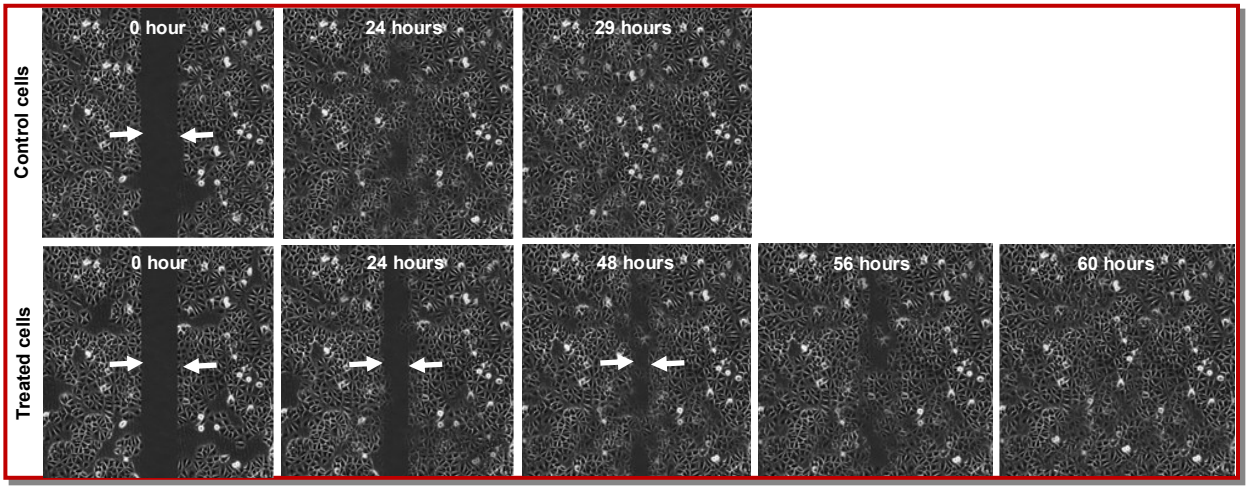

Figure 6: Effect of *L. cylindrica* extract on MCF-7 cell migration in a scratch assay. The images illustrate cell migration at different time points following the creation of a scratch in the monolayer. (Upper row) MCF-7 cells without the extract with images shown at 0, 24, and 29 hours. (Lower row) MCF-7 cells treated with *L. cylindrica* extract with images captured at 0, 24, 48, 56, and 60 hours. Magnification 100x

cells in which the drug was added took 60 hours for the cells to completely cover the scratch made with a sterile micropipette tip (Figure 6). It showed a delayed cell migration in the presence of the extract.

Discussion

The present investigation demonstrates that *L. cylindrica* leaf extract exerts potent, selective cytotoxicity against MCF-7 breast cancer cells while sparing non-tumorigenic MCF-10A cells. Compared with a crude *Catharanthus roseus* extract (IC_{50} >30 µg/mL in MCF-7; selectivity not assessed) (Guan et al., 2021) and *Azadirachta indica* leaf extract (IC_{50} ≈ 25 µg/mL in MCF-7 with concomitant fibroblast toxicity) (Patel et al., 2021), *L. cylindrica* displays equal or superior potency and a markedly higher therapeutic index. Unlike *Withania somnifera* fractions, which trigger apoptosis without migration data (Farooq et al., 2021), the current work integrates both cell-death and anti-migratory assays, revealing a broader anti-cancer profile.

Apoptotic profiling further distinguishes *L. cylindrica* extract. Early phosphatidylserine externalization and chromatin condensation were confirmed via annexin V –FITC and Hoechst/pripodium iodide staining, respectively, extending observations made with *Glycyrrhiza glabra* (annexin V positivity at ~15 µg/mL, without chromatin quantification) (Hameed et al., 2022). In addition, ROS assays indicate that oxidative stress is selectively induced in cancer cells without impairing MCF-10A viability, in contrast to *Camellia sinensis* polyphenols, which reduce ROS but compromise normal epithelial growth (Iqbal et al., 2021).

Synergistic effects likely arise from extracts' rich phenolic and flavonoid composition. HPLC profiling identified quercetin, gallic acid, caffeic acid, benzoic acid, p-coumaric acid, ferulic acid, cinnamic acid, and kaempferol.

Moreover, HPLC analysis revealed additional flavonoid glycosides in the aqueous-ethanol extract, including apigenin 7-o-glucuronide, kaempferide, luteolin O-di-glucoside, neodiosmin, diosmin, and acetylated kaempferol glycosides, underscoring the extract's extensive chemical diversity (Abdel-Salam et al., 2018). Quercetin disrupts PI3K/Akt signaling and activates caspase-3 (Zhou et al., 2021), gallic acid engages both intrinsic and extrinsic apoptotic cascades (Islam et al., 2023), ferulic acid induces G_1 arrest via down-regulation of survival genes (Kang et al., 2024), and cinnamic acid derivatives inflict ROS-mediated DNA damage (Zheng et al., 2008).. Phenolic antioxidants may confer redox homeostasis, provoking lethal oxidative stress preferen-tially in malignant cells.

Anti-migratory activity appears to involve MMP inhibition and cytoskeletal disruption. p-Coumaric acid has been shown to suppress MMP-9 in hepatocellular carcinoma (Tan et al., 2020), while kaempferol down-regulates focal adhesion kinase (Zhou et al., 2021), together accounting for delayed wound closure. Although doxorubicin exhibited lower IC_{50} values in side-by-side testing, its significant toxicity toward MCF -10A cells underscores the favorable safety margin of *L. cylindrica* extract.

In vivo studies and isolation of active fractions will be essential to validate these *in vitro* findings and optimize dosage regimens.

Conclusion

L. cylindrica extract exhibits significant cytotoxic effects

against breast cancer cell lines while sparing normal cells. It induces apoptosis, reduces ROS levels, and inhibits cancer cell migration. These findings highlight its potential as an effective natural anti-cancer agent.

Financial Support

Self-funded

Ethical Issue

The guidelines about the development, acquisition, authentication, cryopreservation, and transfer of cell lines between laboratories were strictly followed. Besides, microbial contamination (commonly mycoplasma), characterization, instability, and misidentification was considered seriously.

Conflict of Interest

Authors declare no conflict of interest

References

Abdel-Salam IM, Ashmawy AM, Hilal AM, Eldahshan OA, Ashour M. Chemical composition of aqueous ethanol extract of *Luffa cylindrica* leaves and its effect on representation of caspase-8, caspase-3, and the proliferation marker Ki67 in intrinsic molecular subtypes of breast cancer *in vitro*. Chem Biodivers. 2018; 15: e1800045.

Alam M, Khan S, Ahmad N. Ethnomedicinal uses and pharmacological properties of *Luffa cylindrica*: A comprehensive review. J Ethnopharmacol. 2023; 295: 115423.

Amin EA, Mohamed RH. FTIR analysis of *Luffa cylindrica* leaf phytochemicals. J Mol Struct. 2021; 1234: 130-37.

Bibi S, Nazir S, Khan A, Zafar, Ali, S. Optimization of UV–Vis spectrophotometric conditions for DPPH assay in herbal matrices. Anal Methods. 2021; 13: 1725-32.

Blois MS. Antioxidant determinations by the use of a stable free radical. Nature 1958; 181: 1199-200.

Bulbul IJ, Zulfiker AH, Hamid K, Khatun MH, Begum Y. Comparative study of *in vitro* antioxidant, antibacterial and cytotoxic activity of two Bangladeshi medicinal plants- *Luffa cylindrica* L. and *Luffa acutangula*. Pharmacogn J. 2011; 3: 59-66.

Duangmano S, Sae-Lim P, Suksamrarn A, Amnuaycheewa S, Shwe M, Padungros S. Cucurbitacin B inhibits human breast cancer cell proliferation through disruption of microtubule polymerization and nucleophosmin B23 translocation. Cancer Biol Ther. 2012; 13: 140-49.

Farooq U, Batool S, Imran M, Sheikh NA, Zafar S. Evaluation of apoptosis using Hoechst 33342 and propidium iodide dual staining. Microsc Res Tech. 2021; 84: 2596-603.

Funmilayo KO, Tolulope OM, Clement AA, Olamide CO, Olalekan LA. Phytochemical profiling (GC-MS and HPLC) and cytotoxicity evaluation of methanol leaf extract of *Luffa cylindrica* on human colon cell lines (HT-29 and HCT-116). J Pharmacogn Phytochem. 2021; 10: 46-53.

Garai S, Ghosh R, Bandopadhyay PP, Mandal NC, Chattopadhyay A. Antimicrobial and anti-cancer properties of echinocystic acid extracted from *Luffa cylindrica*. J Food Process Technol. 2018; 9: 717.

Guan X, Wang S, Liu Y, Lai Z, Huang J, Li C, Zhang Y, Gong X, Deng J, Ye X, Li X. Targeting apoptosis pathways with natural products in cancer therapy: Recent advances. J Ethnopharmacol. 2021; 270: 113806.

Hameed A, Nazir A, Ahmad S, Khan M, Hussain T. Evaluation of apoptosis in breast cancer cells using annexin V-FITC/PI dual staining assay under fluorescence microscopy. Front Cell Dev Biol. 2022; 10: 924735.

Indurthi S, Sarma I. Phytochemicals, bioactive compounds, pharmacologocal effects of *Luffa cylindrica* and their medicinal importance: A review. Plant Arch. 2024; 24: 507-15.

Iqbal J, Ali A, Sarwar T, Khan R, Ahmed Z. DCFDA-based assessment of intracellular reactive oxygen species in cancer cells: Application in oxidative stress studies. Biochim Biophys Acta Gen Subj. 2021; 1865: 129899.

Islam MT, Sarkar C, Rahman MA, Hossain MS, Uddin SJ, Sarker SD. Gallic acid and its derivatives: Promising natural compounds against cancer. J Cell Mol Med. 2023; 27: 1412-25

Kang Y, Wu T, Zhang X, Li Q, Chen J. Ferulic acid inhibits metastasis and epithelial–mesenchymal transition in colorectal cancer via PI3K/Akt pathway modulation. Cancer Chemother Pharmacol. 2024; 93: 123-32.

Khan A, Sultana T, Rahman M. Phytochemical profiling of *Luffa cylindrica* fruit: Identification of phenolic compounds by HPLC. J Ethnopharmacol. 2022; 283: 114713.

Khan A, Sultana T, Rahman M. Standardization of hemocytometer-based cell counting procedures in mammalian cell cultures. Cytotechnology 2021; 73: 761-69.

Liu Y, He L, Li Y. Regulation of apoptosis pathways in tumor progression. Cell Death Dis. 2021; 12: 234.

Nadeem M, Ali A, Farooq M. Cytotoxic and anti-metastatic effects of natural plant extracts on breast cancer cells: A study on *Luffa cylindrica*. J Cancer Res. 2023; 18: 114-22.

Patel H, Desai P, Joshi C. Evaluation of anticancer potential of herbal compounds using trypan blue exclusion and MTT assays in breast cancer cell lines. J Ethnopharmacol. 2021; 267: 113529.

Rahman S, Ali M, Khan A. Optimization of seeding density and incubation time for MTT-based cell viability assays in cancer cell lines. Biomed Methods Protoc. 2022; 5: 45-52.

Rafiq A, Siddiqui M, Ahmed R, Khatri P, Zaman S. Comparative analysis of IC_{50} determination methods for plant extracts. Phytother Res. 2023; 37: 210-17.

Samra, HR. Isolation and characterization of cucurbitacin B from *Luffa cylindrica* and its apoptotic effects on human leukemia cells. Phytother Res. 2018; *32:* 987-95.

Siegel RL, Miller KD, Jemal A. Cancer statistics, 2023. CA

Cancer J Clin. 2023; 73: 17-48.

Sola AO, Oluwagbemileke EA, Adejoke O, Bamikole AO, Ahmad AM. Assessment of phytochemical, antibacterial and antidiabetic properties of extract of *Luffa cylindrica*. Diabetis Manag. 2021; 12: 333-39.

Tan B, Liu X, Zhang Y. p-Coumaric acid inhibits cell proliferation and arrests cell cycle in hepatocellular carcinoma. Oncol Lett. 2020; 20: 2027-34.

Wu Q, Pang X, Ni B, Chen X. Advances in chemotherapy for solid tumours. Oncotarget 2021; 12: 456-68.

Wang H, Li X, Zhang Y. Chemotherapy resistance and cost challenges: Current perspectives. BMC Cancer. 2022; 22: 112.

Zhang Y, Li X, Wang J, Chen H, Zhao M. Standardized protocols for plotting inhibition curves and IC_{50} derivation in antioxidant assays. Food Chem. 2020; 321: 126740.

Zheng L, Dai F, Zhou B, Yang L, Liu Z. Prooxidant activity of hydroxycinnamic acids on DNA damage in the presence of Cu(II) ions: Mechanism and structure-activity relationship. Food Chem Toxicol. 2008; 46: 149-56.

Zhao Y, Xu Z, Wu D. Targeting apoptotic signaling for cancer therapy. Trends Pharmacol Sci. 2020; 41: 130-42.

Zhou L, Wang H, Chen S. Optimization of drying parameters to preserve heat-sensitive phytochemicals in plant extracts. J Pharm Biomed Anal. 2021; 199: 113918.

Author Info

Mohammad Saleem (Principal contact)
e-mail: saleem.pharmacy@pu.edu.pk